Article type : Research Article

Toward real-time verification for MLC tracking treatments using time-resolved EPID imaging

Running title: Real-time verification for MLC tracking

Benjamin J. Zwan[1,2], Vincent Caillet[2,3], Jeremy T. Booth[2,4], Emma Colvill[2,3], Todsaporn Fuangrod[1,5], Ricky O'Brien[3], Adam Briggs[2], Daryl J. O'Connor[1], Paul J. Keall[3], Peter B. Greer[1,6]

[1] School of Mathematical and Physical Sciences, University of Newcastle, Newcastle, NSW, Australia

[2] Northern Sydney Cancer Centre, Royal North Shore Hospital, St Leonards, NSW, Australia

[3] ACRF Image X Institute, School of Physics, University of Sydney, Sydney, NSW, Australia

[4] Institute of Medical Physics, School of Physics, University of Sydney, Sydney, Australia

[5] Faculty of Medicine and Public Health HRH Princess Chulabhorn College of Medical Science, Chulabhorn Royal Academy, Bangkok, Thailand

[6] Department of Radiation Oncology, Calvary Mater Hospital, Newcastle, NSW, Australia

Corresponding author: Benjamin J. Zwan

Mailing address: Northern Sydney Cancer Centre, Reserve Rd, St Leonards, NSW, 2065, AU

Telephone: (02) 94 631378

Email address: Benjamin.Zwan@health.nsw.gov.au

This article has been accepted for publication and undergone full peer review but has not been through the copyediting, typesetting, pagination and proofreading process, which may lead to differences between this version and the Version of Record. Please cite this article as doi: 10.1002/MP.14675

ABSTRACT

Purpose: In multileaf collimator (MLC) tracking, the MLC positions from the original treatment plan are continuously modified to account for intrafraction tumor motion. As the treatment is adapted in real-time there is additional risk of delivery errors which cannot be detected using traditional pre-treatment dose verification. The purpose of this work is to develop a system for real time geometric verification of MLC tracking treatments using an electronic portal imaging device (EPID).

Methods: MLC tracking was utilized during volumetric modulated arc therapy (VMAT). During these deliveries, treatment beam images were taken at 9.57 frames per second using an EPID and frame grabber computer. MLC positions were extracted from each image frame and used to assess delivery accuracy using three geometric measures: the location, size and shape of the radiation field. The EPID-measured field location was compared to the tumor motion measured by implanted electromagnetic markers. The size and shape of the beam were compared to the size and shape from the original treatment plan respectively. This technique was validated by simulating errors in phantom test deliveries and by comparison between EPID-measurements and treatment log files. The method was applied offline to images acquired during the LIGHT SABR clinical trial, where MLC tracking was performed for 17 lung cancer patients. The EPID-based verification results were subsequently compared to post-treatment dose reconstruction.

Results: Simulated field location errors were detected during phantom validation tests with an uncertainty of 0.28 mm (parallel to MLC motion) and 0.38 mm (perpendicular), expressed as a root-mean-square error (RMS_{Error}). For simulated field size errors, the RMS_{Error} was 0.47 cm^2 and field shape changes were detected for random errors with standard deviation $\geq$ 2.5 mm. For clinical lung SABR deliveries, field location errors of 1.6 mm (parallel MLC motion) and 4.9 mm (perpendicular) were measured (expressed as a full-width-half-maximum). The mean and standard deviation of the errors in field size and shape were 0.0±0.3 cm^2 and 0.3±0.1 (expressed as a translation invariant normalized RMS). No correlation was observed between geometric errors during each treatment fraction and dosimetric errors in the reconstructed dose to the target volume for this cohort of patients.

Conclusion: A system for real-time delivery verification has been developed for MLC tracking using time-resolved EPID imaging. The technique has been tested offline in phantom-based deliveries and clinical patient deliveries and was used to independently verify the geometric accuracy of the MLC during MLC tracking radiotherapy.

KEY WORDS: EPID, MLC Tracking, Real-time, Verification, QA

I. INTRODUCTION

In external beam radiotherapy, intrafraction motion of the target can result in a considerable increase in the geometric and dosimetric uncertainty in the delivered dose distribution.[1-6] Traditionally, target motion is accounted for by expanding the margins used for treatment planning to ensure coverage of the target,[1,7] however this results in additional dose to surrounding healthy tissue[3]. This approach also relies on the assumption that the range of the target motion during imaging for treatment planning is reproducible at each treatment fraction. In recent times, efforts have been made to develop systems to compensate for intrafraction motion using real-time adaptation of the treatment delivery. These systems rely on real-time measurement of the target position and subsequent modification of the treatment plan.

Multileaf collimator (MLC) tracking is one such technique where real-time adaptation is achieved by continuously repositioning the beam aperture in response to measured three dimensional (3D) target motion.[8] MLC tracking has been successfully translated into clinical practice to compensate for intrafraction prostate motion[9,10] and respiratory motion of lung tumors[11] during volumetric modulated arc therapy (VMAT). In these studies, 3D target motion was measured using implanted electro-magnetic (EM) transponders and passed to the MLC tracking software which computes modified MLC positions. The modified positions are then sent to the MLC controller in real-time to shift the beam. This technique has been shown to significantly improve the accuracy of the delivered dose distribution and reduce the dose to surrounding healthy tissue and organs at risk.[6,12]

MLC tracking can result in more complex MLC trajectories and introduces additional modes of failure into the delivery. Examples of potential modes of failure include 1) communication issues between the 3D motion measurement device, MLC tracking software and MLC controller, 2) errors within the algorithms of the MLC tracking software (e.g. motion prediction) used to compute new MLC positions and, 3) unexpected latency in the time between motion detection and MLC re-positioning. For conventional radiotherapy, delivery verification is achieved through pre-treatment plan quality assurance (QA). This is problematic for MLC tracking radiotherapy, as the pre-treatment delivery is not the same as the delivered plan at each fraction since the MLC trajectories are adapted and re-optimized in real-time.

QA of MLC tracking deliveries is currently performed before and after treatment delivery.[11] Prior to treatment standard QA methods are employed on the original treatment plan including secondary dose calculation and fluence verification. Additional pre-treatment dose verification is also performed using the Delta4 phantom (ScandiDos, Sweden) with and without patient-specific motion using a HexaMotion stage (ScandiDos, Sweden). Following treatment delivery, dose reconstruction is performed using an isocentre

shift method[13] based on the measured Calypso motion and the treatment log files. There is currently no direct verification of the MLC as part of this QA program and no independent delivery verification during the delivery. As such, errors would not be detected until after the treatment. With SABR being five or fewer fractions, and the demonstration of efficacy of single fraction lung SABR,[14] undetected errors would have a large dosimetric and potentially clinical impact. Ideally the accuracy of the delivery, in particular the MLC, should be verified in real-time using a system which is independent of both the linear accelerator (linac) control system and the MLC tracking software. Furthermore, real-time verification is particularly valuable for MLC tracking as the traditional safety feedback loop between planned and actual MLC positions is not applied by the linac and mechanical limits such as max MLC speed and displacement may not be in effect.[11]

Real-time verification and error detection during external beam radiotherapy have been demonstrated using time-resolved images acquired using an electronic portal imaging device (EPID).[15-17] In these systems, EPID images are continuously acquired during treatment and compared in real-time to predicted EPID images[18] in order to validate the exit fluence transmitted through the patient. Other groups have focused specifically on verifying the MLC trajectories for intensity modulated radiation therapy (IMRT)[16] and VMAT[19,20] and have developed tools which can be applied in real-time. In these methods, MLC positions were extracted from individual EPID frames and compared to the MLC positions from the original treatment plan.

While these methods have been shown to be effective for error detection during conventional IMRT and VMAT, they are not applicable to MLC tracking radiotherapy where the delivery at each fraction is unique. Methods which rely on comparison between measured and predicted exit fluence (e.g. Watchdog) are not practical as the predicted fluence cannot be generated in real-time. Similar issues exist for methods based on MLC verification. In these techniques MLC trajectories can be measured in real-time using EPID imaging, however comparison with MLC positions from the unmodified original treatment plan is not meaningful as these techniques need to be adapted to take actual target motion and tracking into account.

In this work we present a method for real-time geometric verification for MLC tracking treatments using time-resolved EPID imaging. This method was applied to data acquired during LIGHT SABR clinical trial (NCT02514512). The results provided here are the first independent EPID-based validation of the MLC for clinical MLC tracking deliveries.

II. MATERIALS AND METHODS

II.A. Overview of System

Figure 1 provides an overview of the methodology used for real-time verification of MLC tracking treatments. During MLC tracking deliveries transit EPID images are acquired at 9.57 frames-per-second. An independent computer is used to automatically extract the position of each in-field MLC from each EPID frame. The measured MLC positions are then used to perform three verification tests: field location, field size and field shape to validate the MLC during the delivery.

II.B. Delivery Technique and Image Acquisition

All tests were performed using a Varian Trilogy linear accelerator (linac) equipped with a Millennium 120 leaf MLC (Varian Palo Alto, CA, USA). Clinical treatments were planned and delivered using using Varian's RapidArc delivery technique (referred to as VMAT). For MLC tracking, target motion was measured in real-time using trans-bronchially implanted electromagnetic transponders and a room-mounted Varian Calypso tracking system. 3D target motion from Calypso were sent to in-house MLC tracking software. This software computes new MLC positions in real-time and subsequently sends them to the vendor's MLC controller to align the treatment beam with the target position throughout the treatment. The MLC tracking system had an inherent latency of 220 ms that was accounted for using a kernel density estimation prediction algorithm.[21] Additional details regarding the MLC tracking delivery system can be found in previous publications.[10,11]

During each delivery, transmission MV images were continuously acquired using an on-board aS1000 EPID. Individual image frames were collected using an ancillary frame grabber computer and Varian iTools Capture acquisition software. The image frames were then analyzed using software developed in MATLAB (Mathworks, Natick, MA, USA) for delivery verification.

II.C. Extraction of MLC positions

Acquired image frames were first processed to extract the position of each in-field MLC leaf. This methodology has been described in previous studies[19,22] and involves image rotation to account for collimator rotation, compensation for gantry-imager mechanical sag, edge detection and correction for transmission through the curved leaf tip. An additional pre-processing step was applied to the images to account for noise in the EPID image. This noise arises due to interference between radio-frequencies of the Calypso system and the readout electronics of the imaging panel. A modified two-dimensional Butterworth filter was specifically designed to remove the high frequency components of the interference. By performing the above steps for each image frame, the measured MLC positions are known as a function of time and gantry angle throughout the delivery with sub-millimeter accuracy. This

method has been benchmarked in previous publications for static fields[19] and VMAT[19,22] by comparison of EPID-measured MLC positions to positions recorded in machine log files with accuracies of 0.8 mm and 0.2 mm respectively (expressed as one standard deviation).

II.D. Verification Tests

The following sections describe a method developed to verify the MLC aperture during MLC tracking. This method assumes that if the field size and shape should approximately match the original plan and the field is translated to reflect the tumor motion, then the MLC positions are correct. Under this assumption three MLC characteristics are verified for each acquired EPID image frame: field location, field size and field shape.

II.D.1. Field location test

The aim of MLC tracking is to account for target motion by translating the planned MLC-defined aperture to match the instantaneous 3D target motion throughout the delivery. In this method, the actual translation of the EPID-measured MLC aperture is compared to the instantaneous 3D target motion from the Calypso system throughout the delivery. This was done using a rigid image registration technique which is described below and illustrated in Figure 2.

At a particular gantry angle, θ, of a VMAT MLC tracking delivery the original MLC positions from the treatment plan, $MLC_{Plan}(\theta)$, are extracted from the planned control points. Using an EPID image frame acquired at θ the actual MLC positions at θ, $MLC_{EPID}(\theta)$, are measured. Note that these have been modified by the MLC tracking software. Following this the planned and measured MLC positions are converted into a binary fluence image that has pixel values of 1 within the MLC-defined field and values of 0 elsewhere. This conversion is defined by the function, f, in Equation 1. All planned and measured MLC positions are scaled to the treatment isocenter.

$$f(x,y,MLC) = \begin{cases} 1, & for\ pixels\ within\ the\ MLC\ aperture \\ 0, & for\ pixels\ outside\ the\ MLC\ aperture \end{cases} \quad \text{(Equation 1)}$$

Applying this function to $MLC_{Plan}(\theta)$ and $MLC_{EPID}(\theta)$ gives two binary images which are referred to as $I_{Plan}(\theta)$ and $I_{EPID}(\theta)$ respectively. To determine the 2D translation between these two images rigid registration is performed which yields a translation vector with components $\parallel_{EPID}$ and $\perp_{EPID}$ which correspond to shifts parallel and perpendicular to the direction of MLC travel, respectively.

The next step is to determine tumor motion, as measured by the Calypso system, projected onto the plane of the MLC and scaled to the treatment isocenter, referred to as $\parallel_{CAL}$ and $\perp_{CAL}$. These parameters are

computed by projecting the 3D target shift from the Calypso system onto a 2D plane of the MLC defined by the gantry angle, θ. Collimator rotation is also accounted for so that the $\parallel_{CAL}$ and $\perp_{CAL}$ correspond to shifts parallel and perpendicular to the direction of MLC travel. This effectively dissects the 3D target motion into 1D components in the MLC coordinate system (see Supplementary Material 1, Figure S-1). The differences between the measured and predicted field shifts are referred to as $\parallel_{Error}$ (i.e. $\parallel_{EPID} - \parallel_{CAL}$) and $\perp_{Error}$ (i.e. $\perp_{EPID} - \perp_{CAL}$).

II.D.2. Field size test

Field size verification is performed by comparing the measured and planned MLC-defined field area for each EPID image frame. For a given frame, at gantry angle θ, the measured field area, A_{EPID}, is calculated using the MLC positions, $MLC_{EPID}(\theta)$, from the image and known leaf widths. Similarly, the planned MLC positions at θ, $MLC_{Plan}(\theta)$, can be extracted from the control points of the original DICOM plan file to compute the planned field area, A_{Plan}. The field size error during the delivery is defined as the difference between A_{EPID} and A_{Plan}, referred to as A_{Error}.

II.D.3. Field shape test

For each acquired EPID image frame, field shape verification was assessed by generating two binary fluence images, I_{EPID} and I_{Plan}, which are generated using the measured and planned MLC positions respectively. The generation of these images is described in section II.D.1. The similarity between the two shapes was determined using a translation-invariant normalized root-mean-square (S_{RMS}). This metric is defined as the root-mean-square (RMS) error between the two images, which have been translated to maximize the overlap of the images. The resulting RMS error is normalized such that values of S_{RMS} are not dependent on field size. S_{RMS} values close to 1 correspond to poor overlap and a value equal to 0 indicates two identical field shapes. For two registered binary images with dimensions $M \times N$, S_{RMS} is given by Equation 2, where $m = 1, 2,\ldots,M$ and $n = 1, 2,\ldots,N$.

$$S_{RMS} = \frac{\sqrt{\frac{1}{M \times N}\sum_{m,n}[I_{EPID}(m,n) - I_{Plan}(m,n)]^2}}{\sqrt{\frac{1}{M \times N}\sum_{m,n}[I_{EPID}(m,n) + I_{Plan}(m,n)]^2}} \quad \text{(Equation 2)}$$

II.E. In-phantom Validation Tests

The verification software and methodology were validated by performing a series of phantom-based deliveries. As a test case, a typical VMAT lung SABR plan was delivered to an anthropomorphic thorax phantom. The treatment plan was modified to introduce known amounts of changes in field location, field

size and field shape. Field location was varied in the ∥ direction by ±2 mm, ±5 mm and ±10 mm. In the ⊥ direction the field location could only be varied by ±5 mm and ±10 mm with smaller ⊥ shifts not possible due to the finite width of the MLC. This range of magnitudes were chosen as greater magnitudes of errors would result in the MLC aperture being shield by the secondary jaws for this plan. The field size was modified by 0.5 cm^2, 1 cm^2, 2 cm^2 and 3 cm^2. The field shape was varied by introducing random errors into the MLC positions of each control point. The error of each leaf and each control point was randomly sampled from Gaussian function with a specified standard deviation. Plans were generated with different standard deviations (2.5 mm, 5 mm, 7.5 mm and 10 mm) to simulate varying magnitudes of shape distortion. This method was adopted from previous MLC error studies and has shown to correlate with dosimetric errors in the treatment volume.[23] All modified plans were delivered and the acquired EPID images were analyzed using the verification software to determine the accuracy of the verification metrics and the sensitivity of the system as a whole to delivery errors.

For these tests a comparison was also performed between MLC positions extracted from EPID image frames to those recorded in machine log files as an additional validation of the MLC position extraction methodology.

II.F. Patient Tests

The treatment verification system was applied to data acquired during the LIGHT SABR clinical trial (NCT02514512) where intrafraction respiratory lung tumor motion was accounted for using MLC tracking. A total of 30 fractions (spanning over 17 patients) of this trial cohort were analyzed using the delivery verification software. Fractions were only excluded from this study due to incorrect EPID imaging mode or failure to collect all EPID frames. Although the methods presented here were designed to operate in real-time, this analysis was performed offline on the acquired image data. In order to simulate a real-time scenario, the software was restricted to only access information that would be available in a real-time environment, i.e. the image frames, Calypso motion signal and the DICOM plan file.

To understand the importance of the reported errors in field location, size and shape, the dose was reconstructed in the patient's planning CT for each treatment fraction. The Calypso-measured target motion was incorporated into each dose calculation using an isocentre shift method[13] which has been used in a number of previous MLC tracking studies.[6,9-12] The difference between the planned and delivered mean dose (D_{mean}) and dose coverage ($D_{98\%}$) for the gross target volume (GTV) was calculated for each treatment fraction. Note that, a planning treatment volume (PTV) expansion of 5 mm was used to generate each clinical plan in this study. However, for the purpose of evaluating the impact the geometric

uncertainty, the dose to physical tumor volume (i.e. the GTV) was used to assess dose deviations rather than the PTV.

III. RESULTS

III.A. In-phantom Validation Tests

For all phantom test deliveries (19 dual-arc VMAT deliveries in total), the difference between EPID-measured and machine log file MLC positions was -0.02 ± 0.56 mm (-0.84 mm, 0.80 mm), expressed the mean ± standard deviation (5^{th} percentile, 95^{th} percentile).

Table 1 shows the results of the in-phantom validation tests, where MLC errors of known magnitude were introduced into treatment deliveries. The results for an error-free delivery are also tabulated for reference. The RMS_{Error} averaged over all phantom tests was 0.28 mm, 0.38 mm and 0.47 cm2 for ∥ location shifts, ⊥ location shifts and field size changes respectively.

III.B. Examples of Treatment Fractions

Figure 3 shows application of the treatment verification system to three treatment fractions. These fractions were chosen as examples to show how the MLC tracking and verification method performs for different types of tumor motion: (a) motion parallel to the MLC leaf travel (i.e. ∥ direction), (b) motion perpendicular to MLC leaf travel (i.e. ⊥ direction) and (c) irregular high amplitude motion. For each case, the ∥ and ⊥ target motion is plotted from the Calypso system ($\parallel_{CAL}$ and $\perp_{CAL}$) and using the EPID-based field location test ($\parallel_{EPID}$ and $\perp_{EPID}$) which is described in Figure 2. The planned field size, measured field size and the shape similarity are also plotted for the three example cases.

The classification of motion as either ∥ or ⊥ to the MLC depends on the choice of collimator angle. For these deliveries, the collimator angle was set such that the MLC travel direction was aligned to the most dominant tumor motion observed in a pre-treatment 4D-CT. For most patients, the dominant direction of motion was superior-inferior results in a collimator angle of ~90°. For patients with motion dominating in the left-right or anterior-posterior directions a collimator ~0° was used. This aims to minimize the motion perpendicular to the MLC. During VMAT, the amount of ∥ and ⊥ motion will also depend on the gantry angle. The irregular motion in Figure 3 (c), is not specific to a direction but instead refers to high-amplitude non-sinusoidal motion with an inconsistent period.

An example of a typical EPID image frame is given in Figure 4 (a) as well as the corresponding planned MLC aperture. The EPID field location shift and the tumor motion from the Calypso system is plotted for this image in Figure 4 (b). The similarity between the planned and measured aperture shapes for this

image is depicted in Figure 4 (c) which shows the planned aperture overlaid with the EPID aperture after the rigid translation vectors ($\parallel_{EPID}$ and $\perp_{EPID}$) are applied. Figure 4 (d) shows an example of an EPID image and planned MLC aperture for which the shape similarity is relatively poor (S_{RMS} = 0.68). This example image is at a point during the delivery when the tumor is moving perpendicular to direction of MLC motion.

III.C. Overview of delivery accuracy

Figure 5 summarizes the results of the real-time analysis system for all 30 treatment fractions, including 80,000 analyzed EPID image frames. A histogram of the differences in field location in the ∥ and ⊥ directions are shown in (a) and (b) respectively. The full-width-half-maximum (FWHM) of the errors in each direction are $\parallel_{FWHM}$ = 1.6 mm and $\perp_{FWHM}$ = 4.9 mm. The distribution of field size error is shown in Figure 3 (c) which has a mean and standard deviation of 0.0±0.3 cm^2. The shape similarity (S_{RMS}) for all fractions is also displayed as a histogram in Figure 5 (d) which has a mean and standard deviation of 0.3±0.1.

Figure 6 displays (a) the ∥ field location errors, (b) the ⊥ field location errors, (c) the field size errors and (d) the shape similarity for each treatment fraction. The fraction with the largest spread of ∥ location errors in Figure 6 (a) corresponds to the irregular motion example in Figure 3 (c).

III.D. Relationship between dose, accuracy, and motion

The data was analyzed to determine if there was a relationship between the magnitude of tumor motion and the accuracy of each delivery. Here, accuracy of a treatment fraction is represented by the three parameters: RMS location error, RMS field size error, average shape similarity for the fraction. The magnitude of motion was calculated as the standard deviation of the measured motion by the Calypso system in the ∥ and ⊥ direction. Three key correlations were identified and are plotted in Figure 7: (a) ∥ motion versus ∥ location accuracy, (b) ⊥ motion versus ⊥ location accuracy and (c) ⊥ motion and shape similarity. The Pearson Correlation Coefficients (PCC) for the linear fits in (a), (b) and (c) were 0.90 (p-value < 0.0001), 0.65 (p-value < 0.0001) and 0.70 (p-value < 0.0001) respectively. In terms of field size error, there was no significant correlation with magnitude of motion in the ∥ or ⊥ direction.

Figure 8 shows the difference in GTV coverage ($D_{98\%}$) and GTV mean dose (D_{mean}) for each analyzed fraction of this study. All dose differences are expressed as a percentage of the prescribed dose to the target volume. This data was further analyzed to determine if a relationship exists between either $D_{98\%}$ or D_{mean} and the location errors, size errors and shape errors for this patient cohort. No significant

correlations were observed between these dosimetric parameters and the field errors. Details of this investigation are provided in Supplementary Material 2.

IV. DISCUSSION

A system has been developed for real-time delivery verification during MLC tracking deliveries. The methodology was first validated by comparison between EPID-measured MLC positions and machine log files. The standard deviation of the differences between log files and EPID measured positions agrees with previous studies when a phantom is present in the beam.[24] Simulated field location errors in the ∥ and ⊥ direction were detected by the software to within 0.28 mm and 0.38 mm (RMS_{Error}) respectively. The RMS_{Error} between simulated and measured field size errors was 0.47 cm^2. The shape similarity metric, S_{RMS}, was found to be sensitive to Gaussian/random MLC errors with standard deviation $\geq$ 2.5 mm. These results indicate the sensitivity of the methodology to different types of true MLC errors and show uncertainty in MLC position extraction contributes to the uncertainty in the three-verification metrics used in this system.

The verification system was applied to EPID images acquired during MLC tracking treatments for lung cancer patients and is the first independent EPID-based validation of the MLC during clinical MLC tracking deliveries. The accuracy of the delivery system was found to be dependent on the magnitude and direction of the tumor motion relative to the direction of MLC travel, as shown in Figure 3. The FWHM of location errors in the direction perpendicular to the MLC (see Figure 4) was approximately equal to the MLC leaf width which is indicative of leaf-fitting errors.[25] A positive correlation was found between the magnitude of motion and the location accuracy (see Figure 7). Greater motion in the ⊥ direction, resulted in less consistency in shape (Figure 7 (c)), indicating that observed shape errors are at least partially caused by finite leaf speed.

There was no observed correlation between target coverage and delivery accuracy for the 30 fractions included in this study (see Figure 8 and Supplementary Material 2, Table S-2 and Figure S-2). Owing to the difficulties in translating these geometric errors into 3D dose discrepancies in the patient, the EPID-based techniques developed in this work are not intended as a replacement of existing post-treatment dose reconstruction. Rather, it is intended that this new methodology compliments current pre- and post-treatment quality assurance for MLC tracking by offering greater safety during the delivery by real-time detection of gross errors, for example: communication errors, large errors in the motion prediction algorithm and significant systematic MLC positioning errors. The system also has the potential to

supplement real-time 4D dose reconstruction (DoseTracker)[26] where independently measured MLC parameters could be used rather than those recorded by the linac.

A challenge in the future implementation of these methods, is to determine meaningful tolerances and action limits that relate to clinically significant dose constraints in the patient. One approach to this has been developed by Poulsen et al. who showed that the mean area of under-dose and over-dose during an MLC tracking delivery is a good predictor for dosimetric errors within a phantom.[25] Similarly, the dosimetric impact of MLC field size errors during VMAT has been reported[27,28] and can be related to dose errors. Perhaps, the most challenging parameter to relate to dosimetric errors is the field shape. The MLC tracking system uses a leaf optimization algorithm to determine new leaf positions during the delivery based on the measured motion and the finite speed of the MLC leaves. This algorithm seeks to minimize the overdose and underdose of the MLC shape which effectively attempts to preserve the original planned MLC shape that has been shifted to match the target displacement from the isocenter in the beams eye view.[29] Despite this, it is expected that the MLC shape does differ at times during the delivery, even for a non-erroneous delivery due to target localization errors (owing to the motion prediction), leaf-fitting errors (due to the finite leaf width) and leaf adjustment errors (due to MLC speed limitations).[25] An example of this is seen in Figure 4 (d) which shows a visible difference between the planned and delivered MLC field shape. In this instance, the target motion was in a direction perpendicular to the direction of MLC travel and this frame shows an intermediate shape as the target moves beyond half a leaf width in the perpendicular direction.

This inherent uncertainty in shape imposes a limitation in the field location verification methodology as the 2D registration method effectively assumes that tracking system simply translates the planned aperture. This is not the case, as described previously, even if the MLC tracking system is shifting the field location perfectly. This introduces an uncertainty into the image registration process, which is simply put, the uncertainty associated with registering two apertures with shape distortions. The section “Field Location Errors with Field Distortion” in Table 1 quantifies the uncertainty associated with this limitation and can be as high as 2.4 mm (RMS_{Error}) for large amounts of distortion. The uncertainty associated with this effect will vary depending on the type of motion for each patient.

Another practical consideration is that the dosimetric impact of errors may be small if the error only occurs for a short period of time. For example, the dosimetric impact of the example error in field shape in Figure 4 (d) is likely to be insignificant if the shape is corrected in the subsequent image frames acquired. In this case the shape similarity reduces from S_{RMS} = 0.68 to S_{RMS} = 0.2 within 400 ms. Similarly,

for positional errors, an error in a single frame may not translate into a dosimetric impact. This has been investigated in a previous study, where the dosimetric impact of positional errors caused by system latency were assessed.[30] This study showed that 5 mm PTV margins were sufficient to account for up to 500 ms of system latency. If implementing this system practically, a reasonable approach to setting clinically meaningful tolerances may be to include both a temporal and positional criterion. For example, the location error in any direction should not exceed 2.5 mm for more than 500 ms.

The technique presented here are designed to verify the MLC and geometric aspects of the MLC tracking delivery. Other components of the delivery, such as monitor units, are not included in this verification tool as dose rate information is not extracted from the EPID image frames. It is worth noting that the dose rate should be considered when determining the importance of errors. This can be achieved by weighting errors by monitoring units (MU) delivered in the frame. Errors in frames with higher MU per frame will have a larger dosimetric effect. This approach was not applied in this study as, due to the high dose prescribed per fraction, all deliveries had a constant dose rate and MU per frame. MU-weighting of tolerances may be considered if this method is to be applied to treatments in the future with a variable dose rate.

Retrospective assessment of MLC accuracy and dose evaluation has been previously performed using machine log files for conventional radiotherapy and MLC tracking.[6,9,12,13,31,32] While use of log files is efficient and convenient, several studies have shown that they may be insensitive to MLC errors and are not truly independent of the linac control system.[33-35] Agnew et. al.[34] demonstrated that machine log files, were unable to detect systematic MLC positioning errors, for example those caused by miscalibration, mechanical failure of the t-nut, or sub-optimal leaf motor performance. Zwan et. al.[35] showed that log files can be insensitive to errors introduced into the planned MLC positions prior to communication with the MLC controller. Discrepancies greater than 1 mm, between log files and true MLC positions, have also been observed during a clinical delivery.[33] These limitations, stem from the fact that the MLC positions are sourced from the positional encoder attached to each leaf motor and are not a measure of the true radiation field. EPID-based techniques offer a direct measurement of the radiation field edge and hence are sensitive to almost all types of MLC errors and can also be used to validate log files for use in post-treatment dose reconstruction.

While this analysis was performed retrospectively and offline, it was tested in a real-time scenario without using any information that would not be available in a real-time system. The analysis of each image frame could be performed in under 200 ms on a standard computer, so that the verification tests may be

executed five times per second in practice. Future work in this area is to apply this software online in real-time for future MLC tracking trials and clinical implementation.

V. CONCLUSION

A system for real-time delivery verification has been developed for MLC tracking using time-resolved EPID imaging. The technique has been tested in phantom-based deliveries and offline using data acquired during 30 clinical MLC tracking fractions during the LIGHT SABR clinical trial. The geometric delivery accuracy was assessed and reported for these treatments in terms of field location relative to tumor motion, field size and field shape and results were compared with post-treatment dose reconstructions. The system has been developed and tested offline and can be translated to an online real-time environment to be utilized in future clinical trials and during routine clinical use of MLC tracking.

VI. CONFLICTS OF INTEREST

PJK is an inventor on the awarded US patents 7,469,035 and 8,971,489 that are related to MLC tracking. Patent #7,469,035 is unlicensed, patent #8,971,489 has been licensed by the University of Sydney to Leo Cancer Care. JTB (Royal North Shore Hospital) is supported by a Varian Medical Systems Collaborative Research Grant. PJK is supported by an NHMRC Senior Principal Research Fellowship

VII. ACKNOWLEDGEMENTS

The authors thank the patients who enrolled in the LIGHT SABR clinical trial and the team of people involved in acquiring the large amount of data used in the present study. JTB acknowledges support for LIGHT SABR clinical study by a Varian Medical Systems Collaborative Research Grant.

VIII. REFERENCES

1. Keall PJ, Mageras GS, Balter JM, et al. The management of respiratory motion in radiation oncology report of AAPM Task Group 76. *Medical Physics.* 2006;33(10):3874-3898.
2. Huang E, Dong L, Chandra A, et al. Intrafraction prostate motion during IMRT for prostate cancer. *International Journal of Radiation Oncology*Biology*Physics.* 2002;53(2):261-268.
3. George R, Keall PJ, Kini VR, et al. Quantifying the effect of intrafraction motion during breast IMRT planning and dose delivery. *Medical Physics.* 2003;30(4):552-562.
4. Li HS, Chetty IJ, Enke CA, et al. Dosimetric Consequences of Intrafraction Prostate Motion. *International Journal of Radiation Oncology*Biology*Physics.* 2008;71(3):801-812.

5. Adamson J, Wu Q, Yan D. Dosimetric Effect of Intrafraction Motion and Residual Setup Error for Hypofractionated Prostate Intensity-Modulated Radiotherapy With Online Cone Beam Computed Tomography Image Guidance. *International Journal of Radiation Oncology*Biology*Physics.* 2011;80(2):453-461.
6. Colvill E, Poulsen PR, Booth JT, O'Brien RT, Ng JA, Keall PJ. DMLC tracking and gating can improve dose coverage for prostate VMAT. *Medical Physics.* 2014;41(9):091705-n/a.
7. Stroom JC, Heijmen BJ. Geometrical uncertainties, radiotherapy planning margins, and the ICRU-62 report. *Radiotherapy and oncology.* 2002;64(1):75-83.
8. Sawant A, Venkat R, Srivastava V, et al. Management of three-dimensional intrafraction motion through real-time DMLC tracking. *Medical Physics.* 2008;35(5):2050-2061.
9. Colvill E, Booth JT, O'Brien RT, et al. Multileaf Collimator Tracking Improves Dose Delivery for Prostate Cancer Radiation Therapy: Results of the First Clinical Trial. *International Journal of Radiation Oncology*Biology*Physics.* 2015;92(5):1141-1147.
10. Keall PJ, Colvill E, O'Brien R, et al. The first clinical implementation of electromagnetic transponder-guided MLC tracking. *Medical Physics.* 2014;41(2):020702-n/a.
11. Booth JT, Caillet V, Hardcastle N, et al. The first patient treatment of electromagnetic-guided real time adaptive radiotherapy using MLC tracking for lung SABR. *Radiotherapy and Oncology.* 2016;121(1):19-25.
12. Colvill E, Booth J, Nill S, et al. A dosimetric comparison of real-time adaptive and non-adaptive radiotherapy: A multi-institutional study encompassing robotic, gimbaled, multileaf collimator and couch tracking. *Radiotherapy and Oncology.* 2016;119(1):159-165.
13. Poulsen PR, Schmidt ML, Keall P, Worm ES, Fledelius W, Hoffmann L. A method of dose reconstruction for moving targets compatible with dynamic treatments. *Medical Physics.* 2012;39(10):6237-6246.
14. Singh AK, Gomez-Suescun JA, Stephans KL, et al. One versus three fractions of stereotactic body radiation therapy for peripheral stage i to ii non-small cell lung cancer: A randomized, multi-institution, phase 2 trial. *International Journal of Radiation Oncology* Biology* Physics.* 2019;105(4):752-759.
15. Woodruff HC, Fuangrod T, Van Uytven E, et al. First Experience With Real-Time EPID-Based Delivery Verification During IMRT and VMAT Sessions. *International Journal of Radiation Oncology*Biology*Physics.* 2015;93(3):516-522.

16. Todsaporn F, Henry CW, Pejman R, Daryl JOC, Richard HM, Peter BG. An independent system for real-time dynamic multileaf collimation trajectory verification using EPID. *Physics in Medicine & Biology.* 2014;59(1):61.
17. Fuangrod T, Woodruff HC, van Uytven E, et al. A system for EPID-based real-time treatment delivery verification during dynamic IMRT treatment. *Medical Physics.* 2013;40(9):091907-n/a.
18. Chytyk-Praznik K, VanUytven E, Vanbeek T, Greer P, McCurdy B. Model-based prediction of portal dose images during patient treatment. *Medical physics.* 2013;40(3).
19. Zwan BJ, Barnes MP, Fuangrod T, et al. An EPID-based system for gantry-resolved MLC quality assurance for VMAT. *Journal of Applied Clinical Medical Physics.* 2016;17(5):348-365.
20. Bakhtiari M, Kumaraswamy L, Bailey DW, de Boer S, Malhotra HK, Podgorsak MB. Using an EPID for patient-specific VMAT quality assurance. *Medical Physics.* 2011;38(3):1366-1373.
21. Ruan D, Keall P. Online prediction of respiratory motion: multidimensional processing with low-dimensional feature learning. *Physics in Medicine & Biology.* 2010;55(11):3011.
22. Zwan BJ, Barnes MP, Hindmarsh J, et al. Commissioning and quality assurance for VMAT delivery systems: an efficient time-resolved system using real-time EPID imaging. *Medical physics.* 2017;44(8):3909-3922.
23. Oliver M, Gagne I, Bush K, Zavgorodni S, Ansbacher W, Beckham W. Clinical significance of multi-leaf collimator positional errors for volumetric modulated arc therapy. *Radiotherapy and oncology : journal of the European Society for Therapeutic Radiology and Oncology.* 2010;97(3):554-560.
24. Fuangrod T, Woodruff HC, Rowshanfarzad P, O'Connor DJ, Middleton RH, Greer PB. An independent system for real-time dynamic multileaf collimation trajectory verification using EPID. *Physics in Medicine & Biology.* 2013;59(1):61.
25. Poulsen PR, Fledelius W, Cho B, Keall P. Image-based dynamic multileaf collimator tracking of moving targets during intensity-modulated arc therapy. *International Journal of Radiation Oncology* Biology* Physics.* 2012;83(2):e265-e271.
26. Ravkilde T, Skouboe S, Hansen R, Worm E, Poulsen PR. First online real-time evaluation of motion-induced 4D dose errors during radiotherapy delivery. *Medical physics.* 2018;45(8):3893-3903.
27. Oliver M, Gagne I, Bush K, Zavgorodni S, Ansbacher W, Beckham W. Clinical significance of multi-leaf collimator positional errors for volumetric modulated arc therapy. *Radiotherapy and oncology.* 2010;97(3):554-560.
28. Rangel A, Palte G, Dunscombe P. The sensitivity of patient specific IMRT QC to systematic MLC leaf bank offset errors. *Medical Physics.* 2010;37(7):3862-3867.

29. Keall PJ, Sawant A, Cho B, et al. Electromagnetic-guided dynamic multileaf collimator tracking enables motion management for intensity-modulated arc therapy. *International Journal of Radiation Oncology* Biology* Physics.* 2011;79(1):312-320.
30. Bedford JL, Fast MF, Nill S, et al. Effect of MLC tracking latency on conformal volumetric modulated arc therapy (VMAT) plans in 4D stereotactic lung treatment. *Radiotherapy and Oncology.* 2015;117(3):491-495.
31. Kumar MD, Thirumavalavan N, Krishna DV, Babaiah M. QA of intensity-modulated beams using dynamic MLC log files. *Journal of medical physics/Association of Medical Physicists of India.* 2006;31(1):36.
32. Kerns JR, Childress N, Kry SF. A multi-institution evaluation of MLC log files and performance in IMRT delivery. *Radiation Oncology.* 2014;9(1):176.
33. Neal B, Ahmed M, Kathuria K, Watkins T, Wijesooriya K, Siebers J. A clinically observed discrepancy between image-based and log-based MLC positions. *Medical Physics.* 2016;43(6):2933-2935.
34. Agnew A, Agnew C, Grattan M, Hounsell A, McGarry C. Monitoring daily MLC positional errors using trajectory log files and EPID measurements for IMRT and VMAT deliveries. *Physics in Medicine & Biology.* 2014;59(9):N49.
35. Zwan BJ, Hindmarsh J, Seymour E, et al. The dosimetric impact of control point spacing for sliding gap MLC fields. *Journal of Applied Clinical Medical Physics.* 2016;17(6).

Figure 1: Schematic overview of MLC tracking delivery and verification system including real-time measurement of target position (Varian Calypso), modification of MLC positions by the MLC tracking software, EPID image frame acquisition and delivery verification tests.

Figure 2: Schematic description of methodology for field location test. The symbols ∥ and ⊥ refer to translations in field location parallel and perpendicular to the direction of travel of the MLC respectively.

Figure 3: Sample real-time verification results for (a) ∥ direction motion parallel to MLC (b) ⊥ direction motion perpendicular to MLC and (c) high amplitude irregular motion in the ∥ and ⊥ direction.

Figure 4: (a) An example of a typical EPID image frame and the corresponding planned MLC aperture (MLC_{Plan}) from the original DICOM plan file. (b) The computed translation vector from the rigid registration of the measured and planned MLC aperture and the corresponding Calypso-measured tumor motion. (c) The example EPID image with the planned aperture after the translation vectors have been applied ($MLC_{Plan,shift}$). (d) An example of an EPID image and planned MLC aperture with relatively poor shape similarity due to tumor motion in the ⊥ direction.

Figure 5: Distribution of ∥ Location Error, ⊥ Location Error, Shape Similarity and Size Error for all 30 treatment fractions.

Figure 6: Summary of (a) the ∥ field location errors, (b) the ⊥ field location errors (c) the field size errors and (d) the shape similarity for each treatment fraction. Each box and whisker plot shows the median (horizontal line), the inter-quartile range (box) and the 99^{th} percentile (dashed error bar). The vertical solid lines group fractions that correspond to the same patient.

Figure 7: (a) ∥ motion versus ∥ location accuracy, (b) ⊥ motion versus ⊥ location accuracy and (c) ⊥ motion and shape similarity. In each case a linear relationship is fitted to the data.

Figure 8: Summary of target differences between the planned and delivered dose at each fraction in terms of GTV target coverage ($D_{98\%}$) and GTV mean dose (D_{mean}). The vertical solid lines group fractions that correspond to the same patient.

Table 1: Comparison between known (i.e. introduced) errors and detected errors for ‖ location, ⊥ location, field size and field shape errors. For location and size, the mean measured error and the root-mean-square of the difference between the mean and expected error, RMS_{Error}, is tabulated. For field shape, the magnitude of the introduced random error is stated as well as the mean and standard deviation of the shape similarity metric, S_{RMS}. The RMS_{Error} is also given for ‖ and ⊥ field location accuracy for varying degrees of shape distortion (i.e. random MLC error).

‖ Location Errors							
Known Error (mm)	0.0	-10.0	-5.0	-2.0	2.0	5.0	10
Mean Meas. Error (mm)	0.0	-9.9	-4.8	-2.0	2.0	5.0	10.0
RMS_{Error} (mm)	0.0	0.4	0.3	0.2	0.2	0.3	0.4
⊥ Location Errors							
Known Error (mm)	0.0	-10.0	-5.0	-	-	5.0	10.0
Mean Meas. Error (mm)	0.0	-10.0	-5.1	-	-	5.1	10.0
RMS_{Error} (mm)	0.1	0.5	0.5	-	-	0.2	0.4
Field Size Errors							
Known Error (cm^2)	0	0.5	1	2	3		
Mean Meas. Error (cm^2)	0.04	0.56	0.99	2.06	3.03		
RMS_{Error} (mm)	0.48	0.42	0.51	0.48	0.47		
Field Shape Errors							
Stand. Dev. of Known Random Errors (mm)	0	2.5	5	7.5	10		
Mean Shape Sim. (S_{RMS})	0.16	0.32	0.43	0.5	0.56		
Stand. Dev. of Shape Sim. (S_{RMS})	0.04	0.05	0.07	0.07	0.08		
Field Location Errors with Field Distortion							
Stand. Dev. of Known Random Errors (mm)	0	2.5	5	7.5	10		
RMS_{Error} in ‖ Direction (mm)	0.19	0.68	1.25	1.85	2.40		
RMS_{Error} in ⊥ Direction (mm)	0.10	0.10	0.27	0.30	0.90		

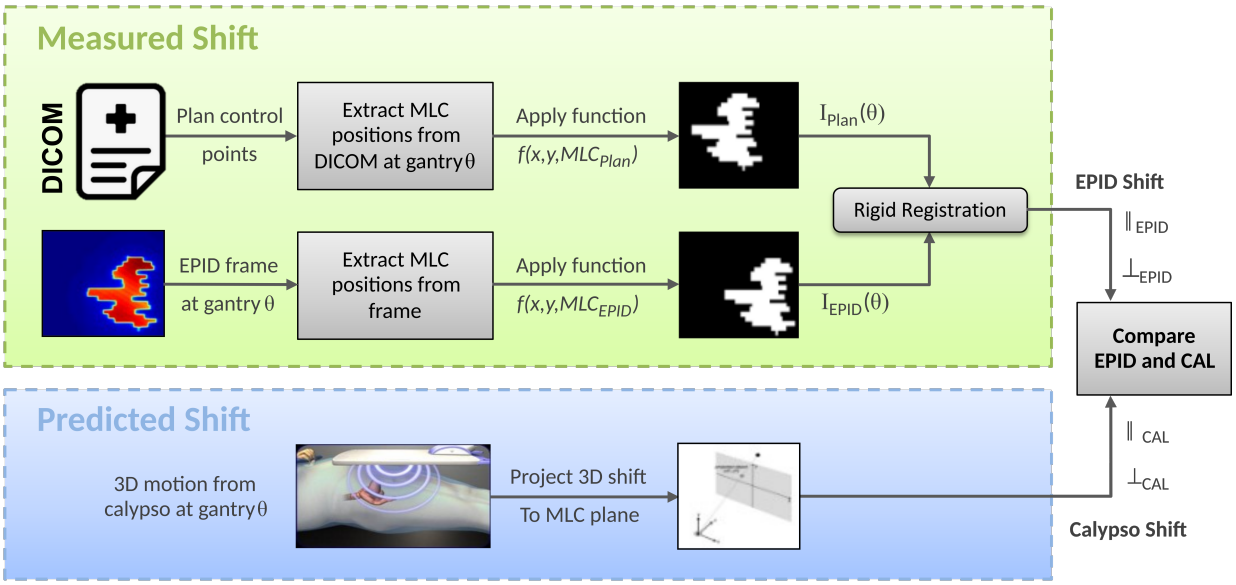

mp_14675_f1.tiff

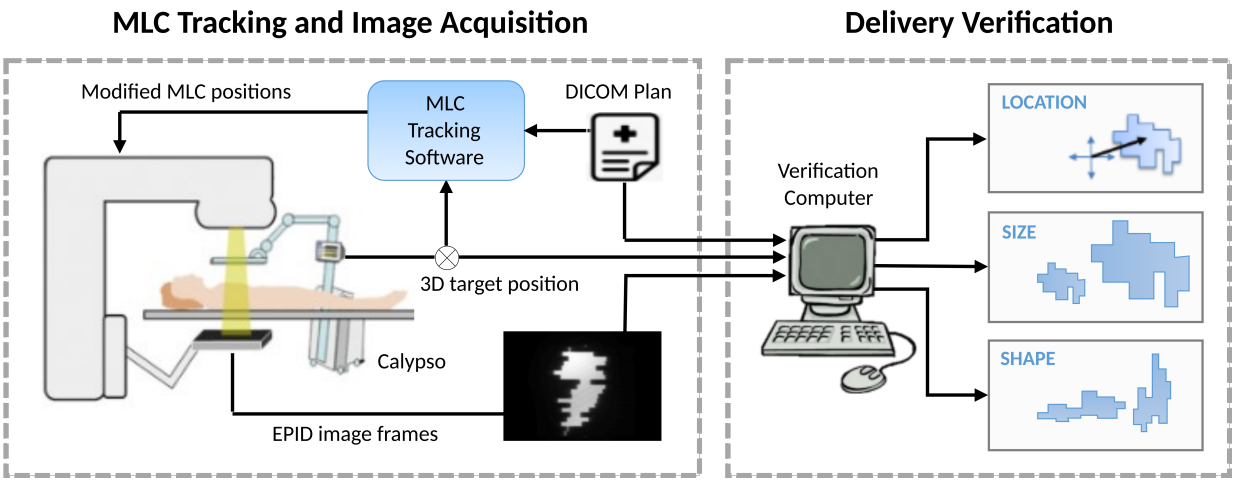

mp_14675_f2.tiff

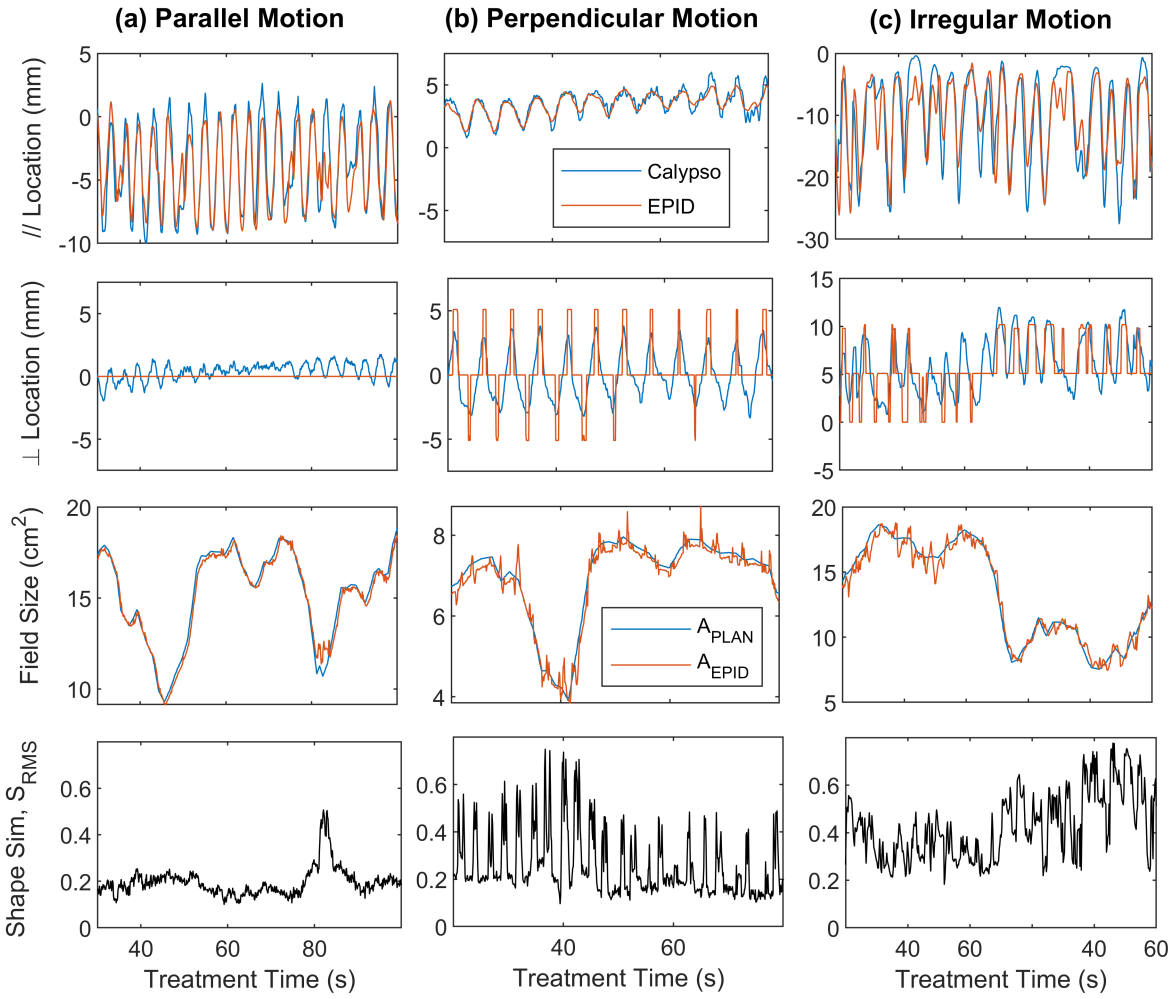

mp_14675_f3.tif

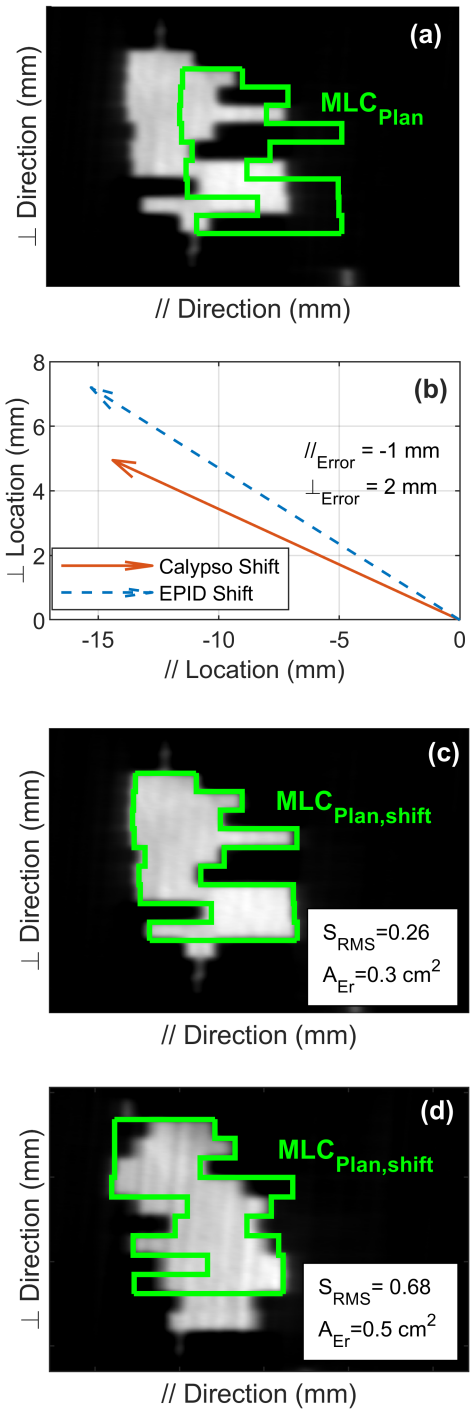

mp_14675_f4.tif

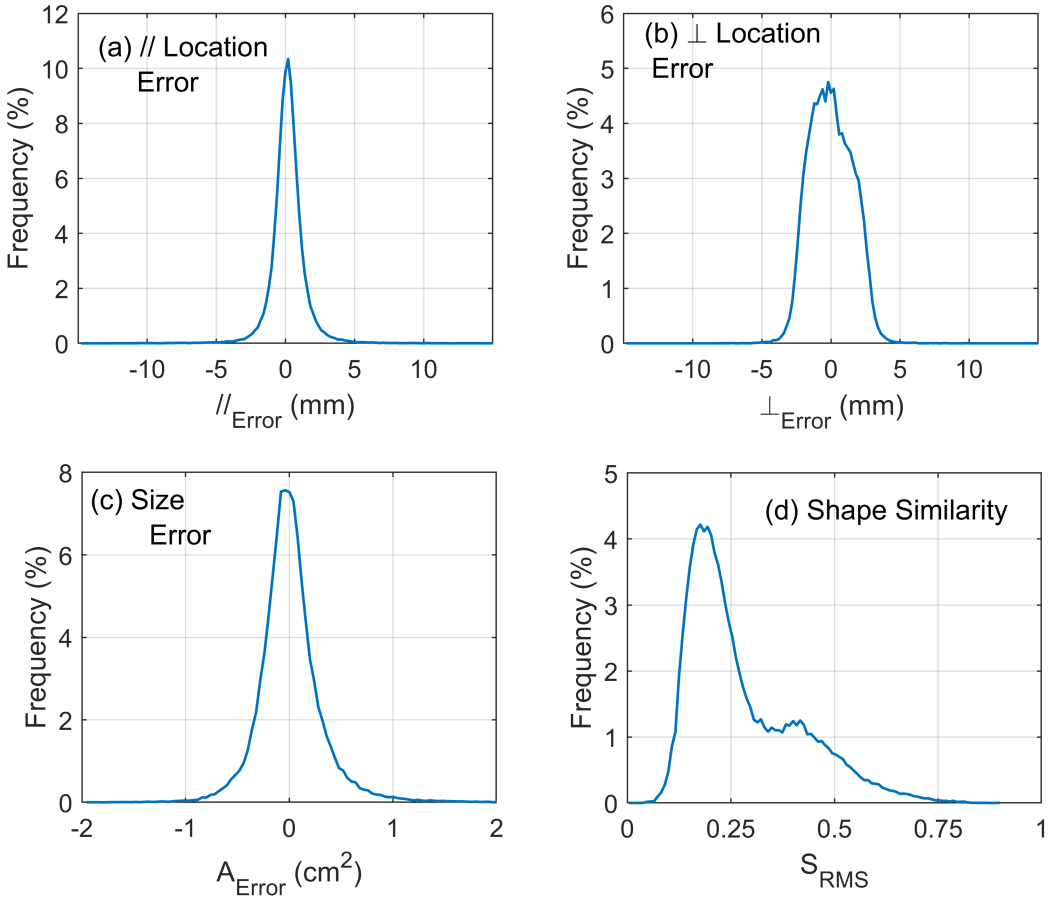

mp_14675_f5.tif

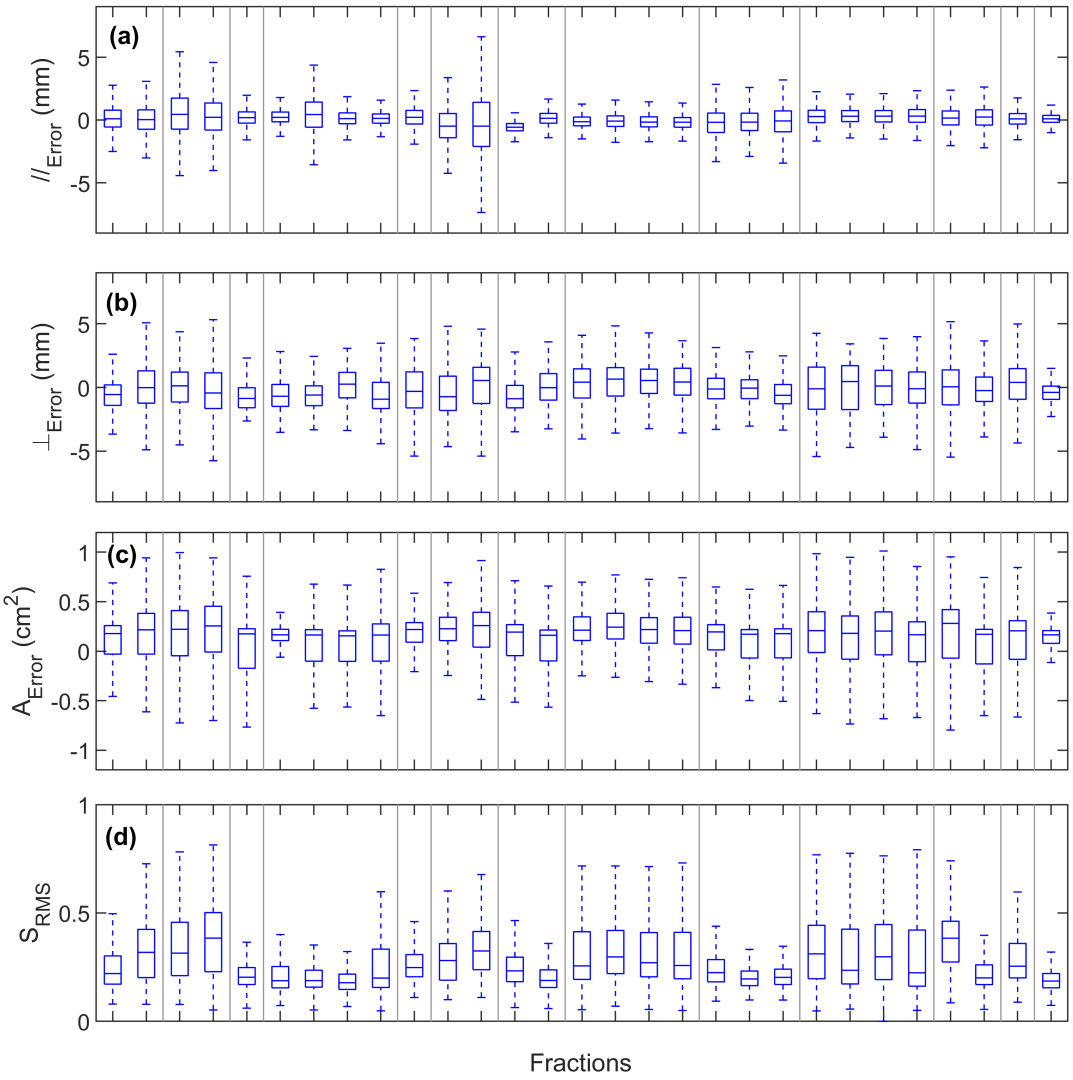

mp_14675_f6.tif

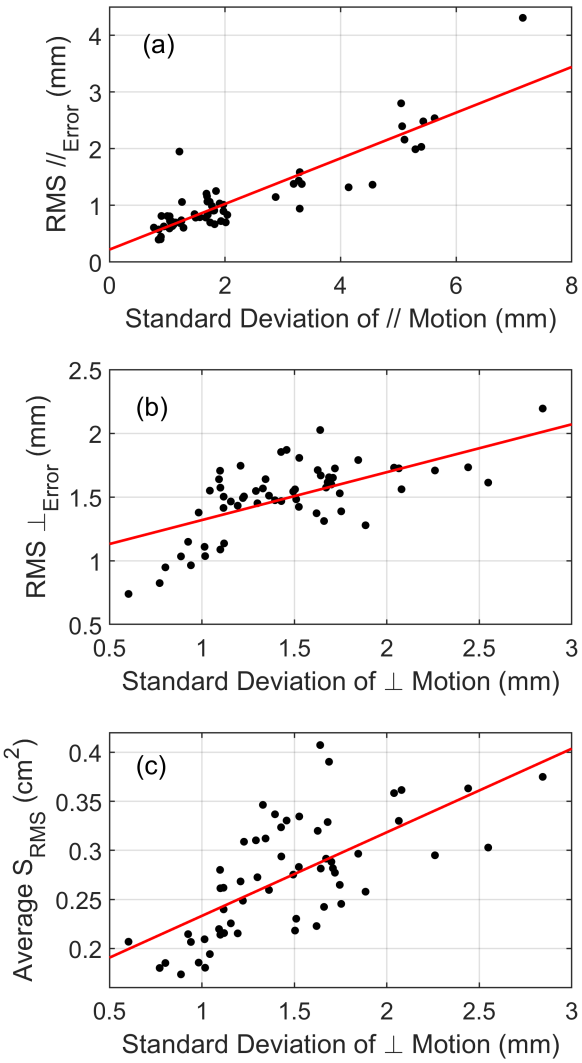

mp_14675_f7.tif

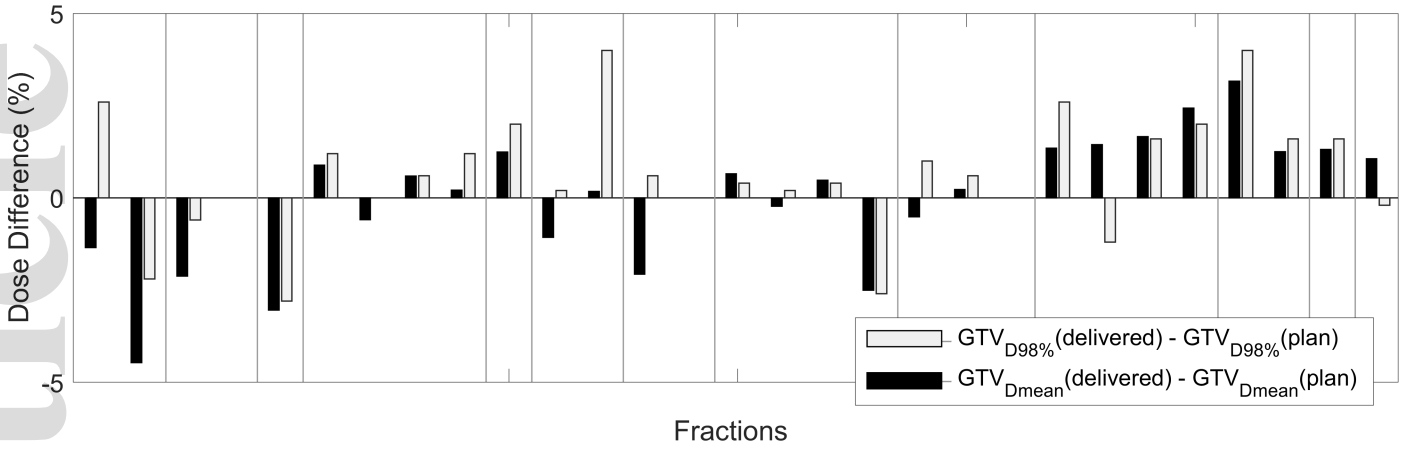

mp_14675_f8.tif